

HAT-P-17b,c: A TRANSITING, ECCENTRIC, HOT SATURN AND A LONG-PERIOD, COLD JUPITER [†]

A. W. HOWARD^{1,2}, G. Á. BAKOS^{3,4}, J. HARTMAN³, G. TORRES³, A. SHPORER⁵, T. MAZEH⁶, GÉZA KOVÁCS⁷,
D. W. LATHAM³, R. W. NOYES³, D. A. FISCHER⁸, J. A. JOHNSON⁹, G. W. MARCY¹, G. A. ESQUERDO³, B. BÉKY³,
R. P. BUTLER¹⁰, D. D. SASSELOV³, R. P. STEFANIK³, G. PERUMPILLY³, J. LÁZÁR¹¹, I. PAPP¹¹, P. SÁRI¹¹

Draft version August 24, 2010

ABSTRACT

We report the discovery of HAT-P-17b,c, a multi-planet system with an inner transiting planet in a short-period, eccentric orbit and an outer planet in a 4.8 yr, nearly circular orbit. The inner planet, HAT-P-17b, transits the bright $V = 10.54$ early K dwarf star GSC 2717-00417, with an orbital period $P = 10.338523 \pm 0.000009$ d, orbital eccentricity $e = 0.346 \pm 0.007$, transit epoch $T_c = 2454801.16945 \pm 0.00020$ (BJD^a), and transit duration 0.1691 ± 0.0009 d. HAT-P-17b has a mass of $0.530 \pm 0.018 M_J$ and radius of $1.010 \pm 0.029 R_J$ yielding a mean density of $0.64 \pm 0.05 \text{ g cm}^{-3}$. This planet has a relatively low equilibrium temperature in the range 780–927 K, making it an attractive target for follow-up spectroscopic studies. The outer planet, HAT-P-17c, has a significantly longer orbital period $P_2 = 1798^{+58}_{-89}$ d and a minimum mass $m_2 \sin i_2 = 1.4^{+1.1}_{-0.4} M_J$. The orbital inclination of HAT-P-17c is unknown as transits have not been observed and may not be present. The host star has a mass of $0.86 \pm 0.04 M_\odot$, radius of $0.84 \pm 0.02 R_\odot$, effective temperature 5246 ± 80 K, and metallicity $[\text{Fe}/\text{H}] = 0.00 \pm 0.08$. HAT-P-17 is the second multi-planet system detected from ground-based transit surveys.

Subject headings: planetary systems — stars: individual (HAT-P-17, GSC 2717-00417) techniques: spectroscopic, photometric

1. INTRODUCTION

With nearly 100 confirmed transiting extrasolar planets (TEPs) known, many studies of planetary properties now focus on the statistical distributions of and correlations between planetary parameters. Individual TEPs still remain extraordinarily valuable, particularly if they have properties that exemplify an important subgroup of planets and orbit stars that are bright enough for meaningful follow-up observations. Such iconic well-studied planets include HD 209458b (Charbonneau et al. 2000; Henry et al. 2000), HD 189733 (Bouchy et al. 2005), GJ 436b (Gillon et al. 2007; Butler et al. 2004), HAT-P-13b,c (Bakos et al. 2010), WASP-12b (Hebb et al. 2009), and GJ 1214b (Charbonneau et al. 2009). The HAT-P-17 system has at least two unusual properties compared

to the ensemble of known TEPs and may serve as an exemplar for planets with these properties. The atmosphere of HAT-P-17b is relatively cool for a TEP and HAT-P-17c is one of only two long-period planets found to orbit a TEP host.

The distribution of TEPs discovered by ground-based transit surveys is biased toward large planets orbiting faint early type stars in short period orbits. Each of these biases stems from the observational selection effects of the surveys that have detected the majority of TEPs: the deep transits of large planets are easier to detect; early type stars dominate magnitude limited surveys; and short-period orbits have higher *a priori* transit probabilities and significantly larger probabilities of detection in a ground-based survey limited to one or two observing sites. The overabundance of detected short period planets has skewed our perception of the atmospheric properties of extrasolar jovian planets. Planets in $P \sim 3$ d orbits ($a \sim 0.04$) experience intense interactions with the radiation and tides of their host stars. The atmospheres of many of these planets are inflated beyond the radii predicted by theoretical models (Fortney et al. 2007). To understand cooler planets, which we know from radial velocity (RV) surveys represent the vast majority of gas giants (Wright et al. 2009), we must study planets orbiting progressively further from their host stars.

With such a scarcity of cool planets, HAT-P-17b is a valuable probe of the planetary mass–radius relationship and additional properties through follow-up observations. Together, the relatively long orbital period and later spectral type of the host star yield an incident stellar flux that is 1–2 orders of magnitude lower than the flux received by most detected TEPs (Kovács et al. 2010). The host star is also relatively

¹ Department of Astronomy, University of California, Berkeley, CA

² Townes Postdoctoral Fellow; howard@astro.berkeley.edu

³ Harvard-Smithsonian Center for Astrophysics, Cambridge, MA; email: gbakos@cfa.harvard.edu

⁴ NSF Fellow

⁵ LCOGT, 6740 Cortona Drive, Santa Barbara, CA, & Department of Physics, Broida Hall, UC Santa Barbara, CA

⁶ School of Physics and Astronomy, Raymond and Beverly Sackler Faculty of Exact Sciences, Tel Aviv University, Tel Aviv 69978, Israel

⁷ Konkoly Observatory, Budapest, Hungary

⁸ Astronomy Department, Yale University, New Haven, CT

⁹ California Institute of Technology, Department of Astrophysics, MC 249-17, Pasadena, CA

¹⁰ Department of Terrestrial Magnetism, Carnegie Institute of Washington, DC

¹¹ Hungarian Astronomical Association, Budapest, Hungary

[†] Based in part on observations obtained at the W. M. Keck Observatory, which is operated by the University of California and the California Institute of Technology. Keck time has been granted by NOAO and NASA.

^a Barycentric Julian dates throughout the paper are calculated from Coordinated Universal Time (UTC)

bright, $V = 10.54$, making follow-up atmospheric studies conceivable. While the *Kepler* mission (Borucki et al. 2010) has been extraordinarily successful in the detection of TEPs, the vast majority of its discovered planets orbit faint stars; only 1.5% of the $\sim 10^5$ stars being surveyed (Batalha et al. 2010) are brighter than 11th magnitude (Kepler magnitude). We predict that HAT-P-17b will be among the small number of well-studied cooler ($T_{\text{eff}} < 1000$ K) TEPs.

Prior to this announcement, only one TEP discovered by a ground-based photometric survey is in a confirmed multi-planet system. HAT-P-13 (Bakos et al. 2010) has a hot Jupiter inner planet and highly eccentric super-Jupiter outer planet with an orbital period of 450 d. The outer planet, HAT-P-13c, was detected only in RV measurements and has not been shown to transit. The system reported here, HAT-P-17, is now the second TEP discovered by a ground-based transit survey with a confirmed second planet. The relatively low rate of detected planet multiplicity among TEPs discovered from by ground may be skewed by the lack of long-term RV and photometric monitoring for most TEP host stars. Measuring the rate of planet multiplicity among stars hosting a hot Jupiter will probe the dynamical histories and migrations mechanisms of hot Jupiters (see, e.g., Wu et al. 2007). Multi-planet systems are significantly more common among RV-detected systems; Wright et al. (2009) find that 28% of known planet host stars are multi-planet systems.

Several multi-planet systems have also been discovered from space. Corot-7 is thought to host two short-period super-Earths (Léger et al. 2009; Queloz et al. 2009), one of which transits. The *Kepler* mission recently announced five candidate systems with multiple transiting planets and is poised to announce additional systems (Steffen et al. 2010).

The Hungarian-made Automated Telescope Network (HATNet; Bakos et al. 2004) survey has been one of the main contributors to the discovery of TEPs. In operation since 2003, it has now covered approximately 14% of the sky, searching for TEPs around bright stars ($8 \lesssim I \lesssim 14.0$). HATNet operates six wide-field instruments: four at the Fred Lawrence Whipple Observatory (FLWO) in Arizona, and two on the roof of the hangar servicing the Smithsonian Astrophysical Observatory’s Submillimeter Array, in Hawaii. Since 2006, HATNet has announced and published 16 TEPs. In this work we report our seventeenth discovery, around the relatively bright star previously known as GSC 2717-00417.

The layout of the paper is as follows. In Section 2 we report the detection of the photometric signal and the follow-up spectroscopic and photometric observations of HAT-P-17. In Section 3 we describe the analysis of the data, beginning with the determination of the stellar parameters, continuing with a discussion of the methods used to rule out nonplanetary, false positive scenarios which could mimic the photometric and spectroscopic observations, and finishing with a description of our global modelling of the photometry and radial velocities. In Section 4 we discuss implications of this discovery, compare our results with recent theoretical models of TEPs, and consider possible follow-on observations.

2. OBSERVATIONS

2.1. Photometric detection

The transits of HAT-P-17b were detected with the HAT-5 telescope in Arizona, the HAT-8 telescope in Hawaii, and with the Wise-HAT (WHAT) telescope at Wise Observatory in Israel (Shporer et al. 2009). The region around GSC 2717-00417, a field internally labeled as 247, was observed on a nightly basis between 2005 May 8 and 2005 October 24, whenever weather conditions permitted. We gathered 9686 exposures of 5 minutes duration at a 5.5 minute cadence. Each image contained approximately 85,000 stars down to $I \sim 14.0$. For the brightest stars in the field, we achieved a per-image photometric precision of 5 mmag. The star is also located in the overlapping field 248, which was observed with the HAT-6 telescope in Arizona and the WHAT telescope in Israel between 2004 June 4 and 2004 November 10, and between 2005 July 3 and 2005 July 15. Altogether 4882 exposures of 5 minutes duration at 5.5 minute cadence were gathered for this field.

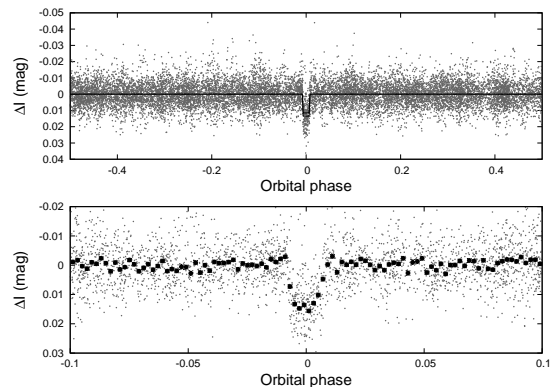


FIG. 1.— Unbinned (top) and binned (bottom) light curves of HAT-P-17 including all 14,000 instrumental I -band 5.5 minute cadence measurements obtained with the HAT-5, HAT-6, and HAT-8 telescopes of HATNet and with the WHAT telescope (see the text for details), and folded with the period $P = 10.3385228$ days (resulting from the global fit described in Section 3). The solid line shows the “P1P3” transit model fit to the light curve (Section 3.3).

The calibration of the HATNet and WHAT frames was carried out using standard photometric procedures. The calibrated images were then subjected to star detection and astrometry, as described in Pál & Bakos (2006). Aperture photometry was performed on each image at the stellar centroids derived from the Two Micron All Sky Survey (2MASS; Skrutskie et al. 2006) catalog and the individual astrometric solutions. The resulting light curves were decorrelated (cleaned of trends) using the External Parameter Decorrelation (EPD; see Bakos et al. 2010) technique in “constant” mode and the Trend Filtering Algorithm (TFA; see Kovács et al. 2005). The light curves were searched for periodic box-shaped signals using the Box Least-Squares (BLS; see Kovács et al. 2002) method. We detected a significant signal in the light curve of GSC 2717-00417 (also known as 2MASS 21380873+3029193 and TYC 2717-417-1; $\alpha = 21^{\text{h}}38^{\text{m}}08.88\text{s}$, $\delta = +30^{\circ}29'19.4''$; J2000; $V=10.54$; Droege et al. 2006), with an apparent depth of ~ 12.0 mmag, and a period of $P = 10.3385$ days (see Figure 1). The drop in brightness had a first-to-last-contact duration, relative to the total period, of

$q = 0.0164 \pm 0.0001$, corresponding to a total duration of $Pq = 4.058 \pm 0.022$ hr (see Figure 1). We note that the transits were only detected from the observations of field 247, and were not detected in the observations of field 248.

2.2. Reconnaissance Spectroscopy

As is routine in the HATNet project, all candidates are subjected to careful scrutiny before investing valuable time on large telescopes. This includes spectroscopic observations at relatively modest facilities to establish whether the transit-like feature in the light curve of a candidate might be due to astrophysical phenomena other than a planet transiting a star. Many of these false positives are associated with large radial-velocity variations in the star (tens of km s^{-1}) that are easily recognized.

One of the tools we have used for this purpose is the Harvard-Smithsonian Center for Astrophysics (CfA) Digital Speedometer (DS; Latham 1992), an echelle spectrograph mounted on the FLWO 1.5 m telescope. This instrument delivers high-resolution spectra ($\lambda/\Delta\lambda \approx 35,000$) over a single order centered on the Mg Ib triplet ($\sim 5187 \text{ \AA}$), with typically low signal-to-noise (S/N) ratios that are nevertheless sufficient to derive radial velocities (RVs) with moderate precisions of $0.5\text{--}1.0 \text{ km s}^{-1}$ for slowly rotating stars. The same spectra can be used to estimate the effective temperature, surface gravity, and projected rotational velocity of the host star, as described by Torres et al. (2002). With this facility we are able to reject many types of false positives, such as F dwarfs orbited by M dwarfs, grazing eclipsing binaries, or triple or quadruple star systems. Additional tests are performed with other spectroscopic observations described in the next section.

For HAT-P-17 we obtained eight observations with the DS between September and November of 2007. The velocity measurements showed an rms residual of 0.60 km s^{-1} , consistent with no detectable RV variation within the precision of the measurements. All spectra were single-lined, i.e., there is no evidence for additional stars in the system. The atmospheric parameters we infer from these observations are the following: effective temperature $T_{\text{eff}\star} = 5250 \pm 125 \text{ K}$, surface gravity $\log g_{\star} = 4.5 \pm 0.25$ (log cgs), and projected rotational velocity $v \sin i = 0.0^{+0.5}_{-0.0} \text{ km s}^{-1}$. The effective temperature corresponds to an early K dwarf star. The mean heliocentric RV of HAT-P-17 is $\gamma_{\text{RV}} = 20.13 \pm 0.21 \text{ km s}^{-1}$.

2.3. High resolution, high S/N spectroscopy

Given the significant transit detection by HATNet, and the encouraging DS results that rule out obvious false positives, we proceeded with the follow-up of this candidate by obtaining high-resolution, high-S/N spectra to characterize the RV variations, and to refine the determination of the stellar parameters. For this we used HIRES (Vogt et al. 1994) on the Keck I telescope located on Mauna Kea, Hawaii, between 2007 October and 2010 April. The width of the spectrometer slit was $0''.86$, resulting in a resolving power of $\lambda/\Delta\lambda \approx 55,000$, with a wavelength coverage of $\sim 3800\text{--}8000 \text{ \AA}$.

We obtained 32 HIRES exposures with an iodine cell mounted directly in front of the spectrometer entrance

slit. The dense set of molecular absorption lines imprinted on the stellar spectra provide a robust wavelength fiducial against which Doppler shifts are measured, as well as strong constraints on the shape of the spectrometer instrumental profile at the time of each observation (Marcy & Butler 1992; Valenti et al. 1995). An additional exposure was taken without the iodine cell, for use as a template in the reductions. Relative RVs in the solar system barycentric frame were derived as described by Butler et al. (1996), incorporating full modeling of the spatial and temporal variations of the instrumental profile. These measurements have typical uncertainties of $1.5\text{--}2.0 \text{ m s}^{-1}$ for spectra with per-pixel signal-to-noise ratios of 100–150. HIRES measurements of late G and early K dwarf stars have achieved long term stability of $1.5\text{--}2.0 \text{ m s}^{-1}$ on standard stars, including noise from systematic and astrophysical sources (Howard et al. 2010). The RV measurements and their uncertainties are listed in Table 1. The period-folded data, along with our best fit described below in Section 3, are displayed in Figure 2.

In the same figure we also show the relative S index, which is a measure of the chromospheric activity of the star derived from the flux in the cores of the Ca II H and K lines. This index was computed following the prescription given by Vaughan, Preston & Wilson (1978), after matching each spectrum to a reference spectrum using a transformation that includes a wavelength shift and a flux scaling that is a polynomial as a function of wavelength. The transformation was determined on regions of the spectra that are not used in Note that our relative S index has not been calibrated to the scale of Vaughan, Preston & Wilson (1978). We do not detect any significant variation of the index correlated with the orbital phase of either planet; such a correlation might have indicated that the RV variations could be due to stellar activity, casting doubt on the planetary nature of the candidates.

In addition, we computed an S_{HK} index calibrated to the Mt. Wilson scale, permitting comparisons with calibrated activity measurements of other stars (Knutson, Howard, & Isaacson 2010). We find $S_{\text{HK}} = 0.162$ (median of all HIRES measurements) and $\log R'_{\text{HK}} = -5.039$ (median). These measurements employ the techniques described in Isaacson & Fischer (2010), calibrated on 1500 stars observed by the California Planet Survey (CPS). We used $B - V = 0.83$ estimated from T_{eff} using the linear transformation between those quantities in Valenti & Fischer (2005).

2.4. Photometric follow-up observations

In order to permit a more accurate modeling of the light curve, we conducted additional photometric observations using a variety of facilities, including: the KeplerCam CCD camera on the FLWO 1.2 m telescope, the 0.6 m Schmidt telescope of Konkoly Observatory at the Pizskéstető Mountain Station, and the 0.46 m and 1.0 m telescopes at Wise Observatory. We observed three transit events of HAT-P-17 with the FLWO 1.2 m telescope on the nights of 2007 December 14, 2008 October 19, and 2009 October 16, while the event on 2008 September 8 was observed simultaneously at Konkoly Observatory and with the two telescopes at Wise Observatory (Figure 3). These observations are summarized in Table 2.

The reduction of these images, including basic cali-

TABLE 1
RELATIVE RADIAL VELOCITIES, BISECTOR SPANS, AND ACTIVITY
INDEX MEASUREMENTS OF HAT-P-17.

BJD (2,454,000+)	RV ^a (m s ⁻¹)	σ_{RV} ^b (m s ⁻¹)	BS (m s ⁻¹)	σ_{BS} (m s ⁻¹)	S ^c
396.82931 ..	18.31	1.62	10.31	4.38	0.0048
397.79661 ..	-8.73	1.63	2.84	5.15	0.0048
427.78145 ..	13.43	1.45	2.49	5.17	0.0047
427.78895	-2.14	5.34	0.0047
429.81978 ..	-46.29	1.62	-3.08	5.46	0.0047
430.84830 ..	-74.61	1.81	-1.88	5.52	0.0046
454.71418 ..	33.26	2.56	-12.71	6.37	0.0048
455.70568 ..	38.42	1.72	0.09	5.13	0.0047
456.69684 ..	37.25	1.84	4.61	4.86	0.0048
457.69351 ..	24.99	1.63	-3.52	5.47	0.0048
603.04188 ..	6.53	1.63	3.60	4.80	0.0047
604.01999 ..	-10.16	1.63	-2.39	5.19	0.0048
638.00747 ..	-80.35	1.56	6.54	4.54	0.0049
640.09696 ..	13.55	1.65	2.73	5.17	0.0048
641.03845 ..	21.59	2.05	9.89	4.28	0.0049
674.90104 ..	7.88	1.90	-15.07	6.42	0.0049
722.81909 ..	5.61	1.76	9.33	4.88	0.0048
726.78740 ..	6.77	1.52	-8.43	5.62	0.0047
727.86651 ..	-13.81	1.89	-5.89	5.34	0.0044
777.87074 ..	11.74	1.61	8.04	4.51	0.0048
778.81597 ..	2.41	1.95	3.34	4.82	0.0049
805.73023 ..	3.20	1.52	9.31	4.65	0.0045
808.77451 ..	6.03	1.43	-3.86	5.37	0.0047
955.07012 ..	-7.96	1.44	5.73	4.54	0.0048
956.08553 ..	-34.98	1.42	1.12	5.07	0.0049
957.07704 ..	-67.81	1.91	-6.36	5.74	0.0048
985.08988 ..	0.05	1.74	1.03	5.04	0.0048
989.04979 ..	-103.08	1.90	-0.24	5.13	0.0047
1043.02166 .	-1.01	1.89	9.50	4.57	0.0048
1106.96789 .	32.17	2.59	-1.47	5.67	0.0048
1192.72802 .	3.26	1.59	-6.09	5.60	0.0050
1198.70293 .	25.65	1.70	2.47	5.18	0.0046
1290.13821 .	-22.07	2.12	-21.11	7.04	0.0045
1319.05702 .	-56.84	2.23	5.54	4.57	0.0046
1319.12199 .	-57.72	2.40	-5.57	5.53	0.0048
1321.12276 .	-20.39	1.37	1.22	5.01	0.0047
1351.97316 .	-26.02	1.50

NOTE. — Note that for the iodine-free template exposures we do not measure the RV but do measure the BS and S index. Such template exposures can be distinguished by the missing RV value.

^a The zero-point of these velocities is arbitrary. An overall offset γ_{rel} fitted to these velocities in Section 3.3 has *not* been subtracted.

^b Internal errors excluding the component of astrophysical jitter considered in Section 3.3.

^c Relative chromospheric activity index, not calibrated to the scale of Vaughan, Preston & Wilson (1978).

TABLE 2
SUMMARY OF PHOTOMETRIC FOLLOW-UP OBSERVATIONS

Facility	Date	Number of Images	Cadence (s)	Filter
KeplerCam/FLWO 1.2 m	2007 Dec 14	367	30	Sloan <i>z</i> -band
Konkoly Schmidt 0.6 m	2008 Sep 8	538	45	<i>I</i> -band
Wise 0.46 m	2008 Sep 8	769	35	<i>R</i> -band
Wise 1.0 m	2008 Sep 8	407	50	<i>R</i> -band
KeplerCam/FLWO 1.2 m	2008 Oct 19	350	33	Sloan <i>i</i> -band
KeplerCam/FLWO 1.2 m	2009 Oct 16	403	33	Sloan <i>i</i> -band

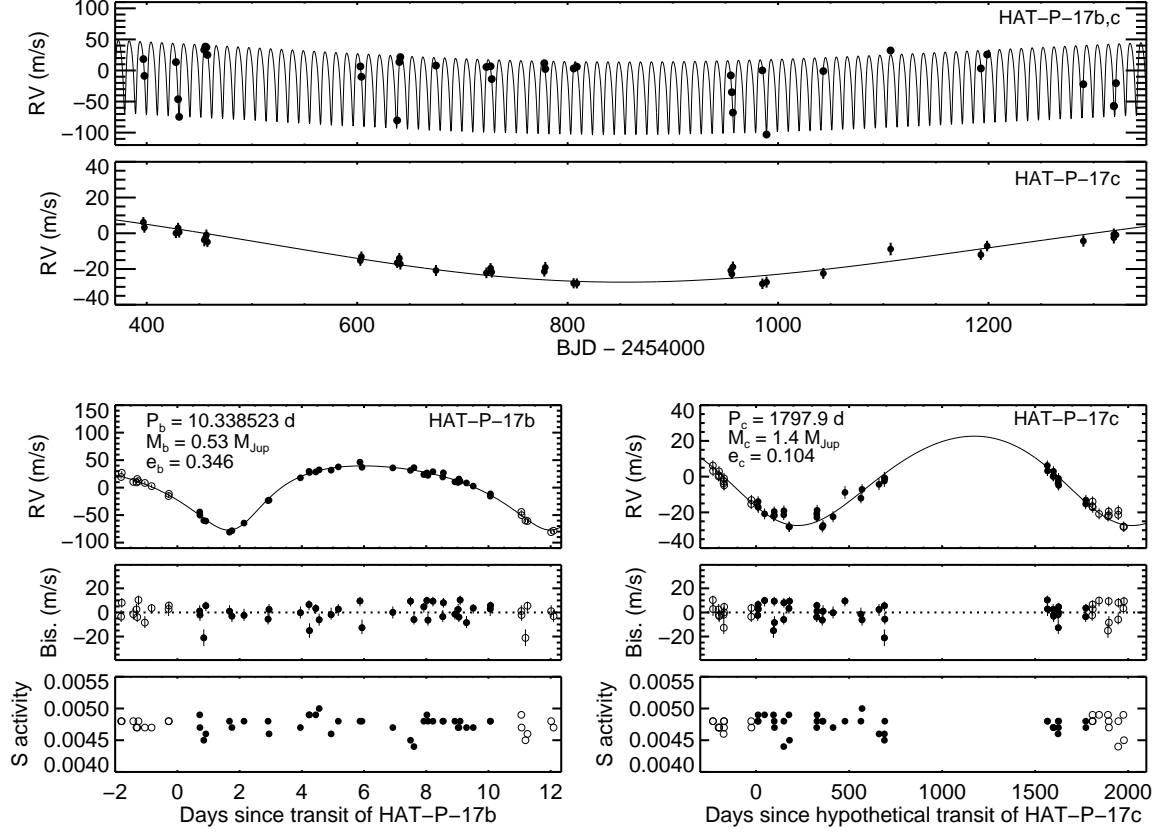


FIG. 2.— *Top*: Keck/HIRES RV measurements for HAT-P-17 shown as a function of BJD, along with our best-fit 2-planet model (see Table 5). The center-of-mass velocity has been subtracted. *Second from top*: Same as top panel except the RV model of the inner planet has been subtracted from the data and the model, revealing the orbit of the outer planet. The rms variation of the residuals to the two-planet model is 3.07 m s^{-1} , requiring a jitter of 2.3 m s^{-1} added in quadrature to the individual errors to yield a reduced χ^2 of 1.0. The error-bars in this panel have been inflated accordingly. *Third row*: RV measurements phased to the orbital periods of the inner planet (left) and the outer planet (right). In each plot the orbit of the other planet has been removed. *Fourth row*: Bisector spans (BS), with the mean value subtracted, phased at the period of the inner planet (left) and the outer planet (right). The measurement from the template spectrum is included (see Section 3.2). *Fifth row*: Relative chromospheric activity index S measured from the Keck spectra, phased at the period of the inner planet (left) and the outer planet (right). Note the different vertical scales of the panels. Observations shown twice are represented with open symbols.

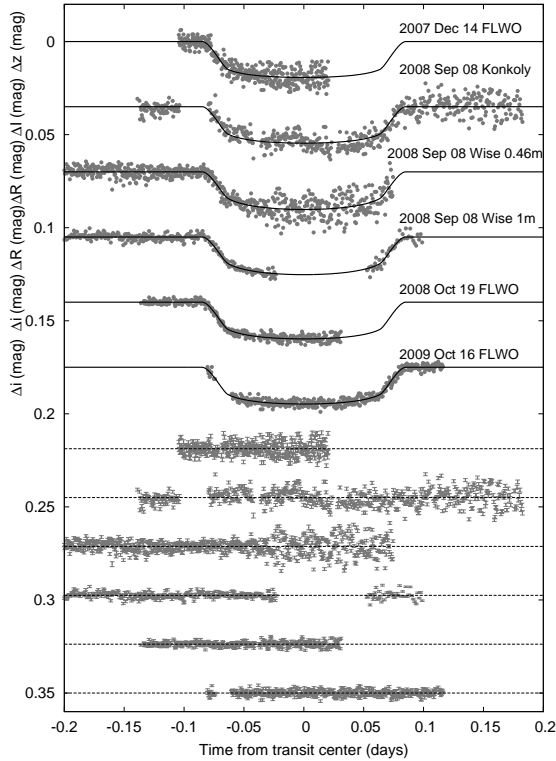


FIG. 3.— Unbinned instrumental z -band, I -band, R -band, and i -band transit light curves, acquired with KeplerCam at the FLWO 1.2 m telescope, with the Schmidt telescope at Konkoly Observatory, and with the 0.46 m and 1 m telescopes at Wise Observatory. The light curves have been EPD- and TFA-processed, as described in § 3.3. The dates and facilities used to observe the events are indicated. Curves after the first are displaced vertically for clarity. Our best fit from the global modeling described in Section 3.3 is shown by the solid lines. Residuals from the fits are displayed at the bottom, in the same order as the top curves. The error bars represent photon and background shot noise, plus readout noise.

bration, astrometry, and aperture photometry, was performed as described by Bakos et al. (2010). We performed EPD and TFA to remove trends simultaneously with the light curve modeling (see Section 3, and Bakos et al. (2010) for details). The final time series are shown in the top portion of Figure 3, along with our best-fit transit light curve model described below; the individual measurements are reported in Table 3.

3. ANALYSIS

3.1. Properties of the parent star

Fundamental parameters of the host star HAT-P-17 such as the mass (M_*) and radius (R_*), which are needed to infer the planetary properties, depend strongly on other stellar quantities that can be derived spectroscopically. For this we have relied on the HIRES template spectrum, and the analysis package known as Spectroscopy Made Easy (SME; Valenti & Piskunov 1996), along with the atomic line database of Valenti & Fischer (2005). SME yielded the following *initial* values and uncertainties (which we have conservatively increased to include our estimates of the systematic errors): effective temperature $T_{\text{eff},*} = 5455 \pm 80$ K, stellar surface gravity $\log g_* = 4.60 \pm 0.10$ (cgs), metallicity $[\text{Fe}/\text{H}] = +0.13 \pm 0.08$ dex, and projected rotational velocity $v \sin i = 0.5 \pm 0.5 \text{ km s}^{-1}$. We adopt the single-sided uncertainty

TABLE 3
HIGH-PRECISION DIFFERENTIAL PHOTOMETRY OF HAT-P-17

BJD (2,400,000+)	Mag ^a	σ_{Mag}	Mag(orig) ^b	Filter
54449.55537	−0.00357	0.00095	9.35242	z
54449.55568	0.00062	0.00094	9.35614	z
54449.55603	−0.00175	0.00095	9.35430	z
54449.55633	0.00203	0.00095	9.35788	z
54449.55668	−0.00602	0.00093	9.35026	z
54449.55700	0.00173	0.00095	9.35703	z
54449.55732	−0.00628	0.00093	9.34882	z
54449.55768	−0.00183	0.00094	9.35300	z
54449.55799	−0.00084	0.00094	9.35409	z
54449.55835	0.00139	0.00093	9.35711	z

NOTE. — This table is available in a machine-readable form in the online journal. A portion is shown here for guidance regarding its form and content.

^a The out-of-transit level has been subtracted. These magnitudes have been subjected to the EPD and TFA procedures, carried out simultaneously with the transit fit.

^b Raw magnitude values without application of the EPD and TFA procedures.

of $\pm 0.5 \text{ km s}^{-1}$ on $v \sin i$ from Valenti & Fischer (2005) based on their SME analysis of nearly 2000 stars. For this star and others with low $v \sin i$, the true error distribution excludes unphysical values ($v \sin i < 0 \text{ km s}^{-1}$) and is likely asymmetric.

In principle the effective temperature and metallicity, along with the surface gravity taken as a luminosity indicator, could be used as constraints to infer the stellar mass and radius by comparison with stellar evolution models. However, the effect of $\log g_*$ on the spectral line shapes is subtle, and as a result it is typically difficult to determine accurately, so that in practice it is a poor luminosity indicator. For planetary transits, a stronger constraint is often provided by a/R_* , the normalized semimajor axis, which is closely related to ρ_* , the mean stellar density. The quantity a/R_* can be derived directly from the transit light curves (see Sozzetti et al. 2007, and also Section 3.3). This, in turn, improves our determination of the spectroscopic parameters by supplying an indirect constraint on the weakly determined spectroscopic value of $\log g_*$ that removes degeneracies. We take this approach here, as described below. The validity of our assumption, namely that the adequate physical model describing our data is a planetary transit (as opposed to a blend), is shown later in Section 3.2.

Our initial values of $T_{\text{eff},*}$, $\log g_*$, and $[\text{Fe}/\text{H}]$ were used to determine auxiliary quantities needed in the global modeling of the follow-up photometry and radial velocities (specifically, the limb-darkening coefficients). This modeling, the details of which are described in Section 3.3, uses a Monte Carlo approach to deliver the probability distribution of a/R_* and other fitted variables. See Pál (2009b) for further details. When combining a/R_* (a luminosity proxy) with assumed Gaussian distributions for $T_{\text{eff},*}$ and $[\text{Fe}/\text{H}]$ from SME, we compare with stellar evolution models to estimate the probability distributions of additional inferred stellar parameters, including $\log g_*$. Here we use the stellar evolution calculations from the Yonsei-Yale (YY) series by Yi et al. (2001). The comparison with the model isochrones was carried out for each of 20,000 Monte Carlo trial sets (see Section 3.3). Parameter combinations corresponding to

unphysical locations in the H-R diagram (1.5% of the trials) were ignored, and replaced with another randomly drawn parameter set. The result and error estimate for the surface gravity, $\log g_\star = 4.53 \pm 0.02$, is different from the result of our initial SME analysis, which is not surprising in view of the strong correlations among $T_{\text{eff}\star}$, $[\text{Fe}/\text{H}]$, and $\log g_\star$ that are often present in spectroscopic determinations. Therefore, we carried out a second iteration in which we adopted this value of $\log g_\star$ and held it fixed in a new SME analysis (coupled with a new global modelling of the RV and light curves), adjusting only $T_{\text{eff}\star}$, $[\text{Fe}/\text{H}]$, and $v \sin i$. This gave $T_{\text{eff}\star} = 5246 \pm 80$ K, $[\text{Fe}/\text{H}] = 0.00 \pm 0.08$, and $v \sin i = 0.3 \pm 0.5 \text{ km s}^{-1}$, in which the conservative uncertainties for the first two have been increased by a factor of two over their formal values, as before. A further iteration did not change $\log g_\star$ significantly, so we adopted the values stated above as the final atmospheric properties of the star. They are collected in Table 4, together with the adopted values for the macroturbulent and microturbulent velocities.

With the adopted spectroscopic parameters the model isochrones yield the stellar mass and radius, $M_\star = 0.857 \pm 0.039 M_\odot$ and $R_\star = 0.837 \pm 0.021 R_\odot$, along with other properties listed at the bottom of Table 4. HAT-P-17 is a early K dwarf star with an estimated age of 7.8 ± 3.3 Gyr, according to these models. The inferred location of the star in a diagram of a/R_\star versus $T_{\text{eff}\star}$, analogous to the classical H-R diagram, is shown in Figure 4. The stellar properties and their 1σ and 2σ confidence ellipsoids are displayed against the backdrop of Yi et al. (2001) isochrones for the measured metallicity of $[\text{Fe}/\text{H}] = 0.00$, and a range of ages. For comparison, the location implied by the initial SME results is also shown (triangle).

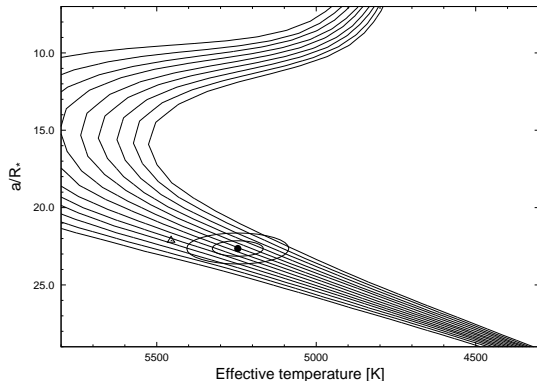


FIG. 4.— Model isochrones from Yi et al. (2001) for the measured metallicity of HAT-P-17, $[\text{Fe}/\text{H}] = 0.00$, and ages between 1.0 and 13.0 Gyr with a step-size of 1.0 Gyr (left to right). The adopted values of $T_{\text{eff}\star}$ and a/R_\star are shown together with their 1σ and 2σ confidence ellipsoids. The initial values of $T_{\text{eff}\star}$ and a/R_\star from the first SME and light curve analyses are represented with a triangle.

The stellar evolution modelling provides color indices that may be compared against the measured values as a sanity check. The best available measurements are the near-infrared magnitudes from the 2MASS Catalogue (Skrutskie et al. 2006), $J_{2\text{MASS}} = 9.017 \pm 0.022$, $H_{2\text{MASS}} = 8.619 \pm 0.029$ and $K_{2\text{MASS}} = 8.544 \pm 0.025$; which we have converted to the photometric system of the models (ESO system) using the transformations by

TABLE 4
STELLAR PARAMETERS FOR HAT-P-17

Parameter	Value	Source
Spectroscopic properties		
$T_{\text{eff}\star}$ (K)	5246 ± 80	SME ^a
$[\text{Fe}/\text{H}]$	0.00 ± 0.08	SME
$v \sin i$ (km s^{-1})	0.3 ± 0.5	SME
v_{mac} (km s^{-1})	3.21	SME
v_{mic} (km s^{-1})	0.85	SME
γ_{RV} (km s^{-1})	20.13 ± 0.21	DS
Photometric properties		
V (mag)	10.54	TASS
$V - I_C$ (mag)	0.901 ± 0.10	TASS
J (mag)	9.017 ± 0.022	2MASS
H (mag)	8.619 ± 0.029	2MASS
K_s (mag)	8.544 ± 0.025	2MASS
Derived properties		
M_\star (M_\odot)	0.857 ± 0.039	YY+ a/R_\star +SME ^b
R_\star (R_\odot)	0.837 ± 0.021	YY+ a/R_\star +SME
$\log g_\star$ (cgs)	4.53 ± 0.02	YY+ a/R_\star +SME
L_\star (L_\odot)	0.48 ± 0.04	YY+ a/R_\star +SME
M_V (mag)	5.75 ± 0.12	YY+ a/R_\star +SME
M_K (mag, ESO)	3.79 ± 0.07	YY+ a/R_\star +SME
Age (Gyr)	7.8 ± 3.3	YY+ a/R_\star +SME
Distance (pc)	90 ± 3	YY+ a/R_\star +SME

^a SME = “Spectroscopy Made Easy” package for the analysis of high-resolution spectra (Valenti & Piskunov 1996). These parameters rely primarily on SME, but have a small dependence also on the iterative analysis incorporating the isochrone search and global modelling of the data, as described in the text.

^b YY+ a/R_\star +SME = Based on the YY isochrones (Yi et al. 2001), a/R_\star as a luminosity indicator, and the SME results.

Carpenter (2001). The resulting measured color index is $J - K = 0.504 \pm 0.036$. This is within 1σ of the predicted value from the isochrones of $J - K = 0.53 \pm 0.02$. The distance to the object may be computed from the absolute K magnitude from the models ($M_K = 3.79 \pm 0.07$) and the 2MASS K_s magnitude, which has the advantage of being less affected by extinction than optical magnitudes. The result is 90 ± 3 pc, where the uncertainty excludes possible systematics in the model isochrones that are difficult to quantify.

3.2. Spectral line-bisector analysis

Our initial spectroscopic analyses discussed in Section 2.2 and Section 2.3 rule out the most obvious astrophysical false positive scenarios. However, more subtle phenomena such as blends (contamination by an unresolved eclipsing binary, whether in the background or associated with the target) can still mimic both the photometric and spectroscopic signatures we see.

Following Torres et al. (2007), we explored the possibility that the measured radial velocities are not the results of a planet in Keplerian motion, but are instead caused by distortions in the spectral line profiles due to contamination from a nearby unresolved eclipsing binary. A bisector analysis based on the Keck spectra was done as described in §5 of Bakos et al. (2007). We detect no variation in excess of the measurement errors in the bisector spans (see Figure 2). The correlation between the radial velocities and the bisector variations is insignificant. Therefore, we conclude that the velocity variations are real, and that the star is orbited by a close-in giant planet.

3.3. Global modelling of the data

This section describes the procedure we followed to model the HATNet photometry, the follow-up photometry, and the radial velocities simultaneously. Our model for the follow-up light curves used analytic formulae based on Mandel & Agol (2002) for the eclipse of a star by a planet, with limb darkening being prescribed by a quadratic law. The limb darkening coefficients for the I , R and Sloan z and i bands were interpolated from the tables by Claret (2004) for the spectroscopic parameters of the star as determined from the SME analysis (Section 3.1). The transit shape was parametrized by the normalized planetary radius $p \equiv R_p/R_*$, the square of the impact parameter b^2 , and the reciprocal of the half duration of the transit ζ/R_* . We chose these parameters because of their simple geometric meanings and their negligible correlations with each other (see Bakos et al. 2010). The relation between ζ/R_* and the quantity a/R_* , used in Section 3.1, is given by

$$a/R_* = P/2\pi(\zeta/R_*)\sqrt{1-b^2}\sqrt{1-e^2}/(1+e\sin\omega) \quad (1)$$

(see, e.g., Tingley & Sackett 2005). Our model for the HATNet data was the simplified “P1P3” version of the Mandel & Agol (2002) analytic functions (an expansion in terms of Legendre polynomials), for the reasons described in Bakos et al. (2010).

Initial modelling of the RV observations showed deviations from a Keplerian fit highly suggestive of a second body in the system with a much longer period than the transiting planet. Thus, in our global modelling, the RV curve was parametrized by the combination of an eccentric Keplerian orbit for the inner planet with semi-amplitude K , and Lagrangian orbital elements $(k, h) \equiv e \times (\cos\omega, \sin\omega)$, plus an eccentric Keplerian orbit for the outer object with K_2 , k_2 and h_2 , and a systemic RV zero-point γ (see also Bakos et al. 2010). Throughout this paper the subscripts “1” and “2” refer to HAT-P-17b and HAT-P-17c, respectively. If the subscript is omitted, we refer to HAT-P-17b.

We assumed a strict periodicity in the individual transit times. We assigned the transit number $N_{tr} = 0$ to the last complete follow-up light curve gathered on 2009 Oct 16. The adjustable parameters in the fit that determine the ephemeris were chosen to be the time of the first transit center observed with HATNet, $T_{c,-65}$, and that of the last transit center observed with the FLWO 1.2 m telescope, $T_{c,0}$. We used these as opposed to period and reference epoch in order to minimize correlations between parameters (see Pál et al. 2008). Times of mid-transit for intermediate events were interpolated using these two epochs and the corresponding transit number of each event, N_{tr} . The eleven main parameters describing the physical model were thus $T_{c,-65}$, $T_{c,0}$, R_p/R_* , b^2 , ζ/R_* , K , $k \equiv e \cos\omega$, $h \equiv e \sin\omega$, K_2 , k_2 and h_2 . Five additional parameters were included that have to do with the instrumental configuration. These are the HATNet blend factor $B_{\text{inst},247}$, and $B_{\text{inst},248}$ which accounts for possible dilution of the transit in the 247 and 248 HATNet light curves from background stars due to the broad PSF (20'' FWHM), the HATNet out-of-transit magnitudes $M_{0,\text{HATNet},247}$, and $M_{0,\text{HATNet},248}$, and the relative zero-point γ_{rel} of the Keck RVs.

We extended our physical model with an instrumental

model that describes brightness variations caused by systematic errors in the measurements. This was done in a similar fashion to the analysis presented by Bakos et al. (2010). The HATNet photometry has already been EPD- and TFA-corrected before the global modeling, so we only considered corrections for systematics in the follow-up light curves. We chose the “ELTG” method, i.e., EPD was performed in “local” mode with EPD coefficients defined for each night, and TFA was performed in “global” mode using the same set of stars and TFA coefficients for all nights. The total number of fitted parameters was 16 (physical model with 5 configuration-related parameters) + 36 (local EPD) + 10 (global TFA) = 67, i.e. much smaller than the number of data points (2866, counting only RV measurements and follow-up photometry measurements).

The joint fit was performed as described in Bakos et al. (2010). We minimized χ^2 in the space of parameters using a hybrid algorithm, combining the downhill simplex method (AMOEBA; see Press et al. 1992) with a classical linear least squares algorithm. Parameter uncertainties were derived applying the Markov Chain Monte-Carlo method (MCMC, see Ford 2006) using “Hyperplane-CLLS” chains (Bakos et al. 2010). This provided the full *a posteriori* probability distributions of all adjusted variables. The *a priori* distributions of the parameters for these chains were chosen to be Gaussian, with eigenvalues and eigenvectors derived from the Fisher covariance matrix for the best-fit solution. The Fisher covariance matrix was calculated analytically using the partial derivatives given by Pál (2009).

Following this procedure we obtained *a posteriori* distributions for all fitted variables, and other quantities of interest such as a/R_* . As described in Section 3.1, a/R_* was used with stellar evolution models to infer a theoretical value for $\log g_*$ that is significantly more accurate than the spectroscopic value. The improved estimate was in turn applied to a second iteration of the SME analysis, as explained previously, to obtain better estimates of $T_{\text{eff},*}$ and $[\text{Fe}/\text{H}]$. The global modeling was then repeated with updated limb-darkening coefficients based on those new spectroscopic determinations. The resulting geometric parameters pertaining to the light curves and velocity curves are listed in Table 5 and Table 6.

Included in Table 5 is the RV “jitter”. This quantity accounts for RV variability due to rotational modulation of stellar surface features, stellar pulsation, undetected planets, and uncorrected systematic errors in the velocity reduction (Wright 2005). Our adopted jitter value of 2.3 ms^{-1} was chosen so that reduced $\chi^2 = 1$ for the RV data of the global fit. This value is consistent with the jitter of an ensemble of chromospherically quiet, late G/early K dwarf stars (Wright 2005). Auxiliary parameters not listed in the tables are: $T_{c,-65} = 2454449.65967 \pm 0.00035$ (BJD), $T_{c,0} = 2455121.66365 \pm 0.00034$ (BJD), the blending factors $B_{\text{instr},247} = 0.87 \pm 0.04$ and $B_{\text{instr},248} = 0.69 \pm 0.16$, and $\gamma_{\text{rel}} = 25.0 \pm 7.6 \text{ m s}^{-1}$. The latter quantity represents an arbitrary offset for the Keck RVs, and does *not* correspond to the true center of mass velocity of the system, which was listed earlier in Table 4 (γ_{RV}).

The planetary parameters and their uncertainties are derived from the *a posteriori* distributions of the stel-

lar, light curve, and RV parameters. We find an inner planet mass of $M_p = 0.530 \pm 0.018 M_J$ and a radius of $R_p = 1.010 \pm 0.029 R_J$, giving a mean density $\rho_p = 0.64 \pm 0.05 \text{ g cm}^{-3}$. These and other planetary parameters are listed at the bottom of Table 5. We note that the inner planets's eccentricity is significantly non-zero: $e = 0.346 \pm 0.007$, $\omega = 201 \pm 2^\circ$.

In addition to HAT-P-17b, we detect a second, outer planet in the system. HAT-P-17c is a long-period jovian planet with a minimum mass $m_2 \sin i_2 = 1.4^{+1.1}_{-0.4} M_J$ and orbital period $P_2 = 1798^{+58}_{-89}$ days. Its eccentricity of $e_2 = 0.10^{+0.23}_{-0.10}$ is consistent with a circular orbit. Because we have only measured about half of an orbit of HAT-P-17c, we conservatively adopt 95.4% confidence intervals ('2- σ errors') for the error estimates on parameters associated with this planet. (Unless noted, all other parameter uncertainties in this paper are 68.3% confidence intervals, '1- σ errors'.) Figure 5 shows the distributions of and correlations between $m_2 \sin i_2$, P_2 , and e_2 from the MCMC analysis. Correlations between the Lagrangian orbital parameters $k_2 = e_2 \cos \omega_2$ and $h_2 = e_2 \sin \omega_2$ are also shown.

4. DISCUSSION

We present the detection of HAT-P-17b, a transiting hot Saturn in an eccentric orbit, and HAT-P-17c, a cold Jupiter near the ice line with an unknown orbital inclination. In this section we discuss these two planets in the context of recent models and trends, the statistics of nearly 100 TEPs, and the small number of multi-planet systems with one or more transiting members.

4.1. The Planet HAT-P-17b

As seen in Figure 6, HAT-P-17b has a radius that is typical of other known TEPs with masses in the range 0.5–0.6 M_J . Comparing HAT-P-17b to the theoretical models by Fortney et al. (2007) we find that it is consistent with gas-dominated planet having a core-mass of $M_C \sim 25 M_\oplus$ for an age of 4 Gyr, or somewhat less than this for older ages. HAT-P-17b is not inflated relative to theoretical models. This lack of inflation is consistent with the relatively cool temperature ($T_{\text{eq}} = 792 \pm 15 \text{ K}$) of HAT-P-17b.

4.1.1. A Predicted Non-inverted Atmosphere?

Secondary eclipse measurements of TEPs in multiple passbands with the *Spitzer Space Telescope* have revealed two classes of atmospheres among jovian planets. “Non-inverted” atmospheres are described well by 1D atmospheric models with water in absorption. In contrast, “inverted” atmospheres show dayside emission spectra that are best modeled by a high-altitude temperature inversion and water in emission. Physically, such an inversion requires a high-altitude absorber. Planets in intermediate states (mild inversions, etc) also appear possible. Knutson, Howard, & Isaacson (2010) noted that planets with inverted atmospheres systematically orbit chromospherically quiet stars while planets with non-inverted atmospheres orbit chromospherically active stars. They proposed that chromospheric activity, as measured by the Ca II H & K index $\log R'_{\text{HK}}$, traces UV flux which is responsible for destroying the photochemically labile inversion-causing molecules. These authors are agnostic

TABLE 5
ORBITAL AND PLANETARY PARAMETERS FOR HAT-P-17B

Parameter	Value
Light curve parameters	
P (days)	10.338523 \pm 0.000009
T_c (BJD) ^a	2454801.16945 \pm 0.00020
T_{14} (days) ^a	0.1691 \pm 0.0009
$T_{12} = T_{34}$ (days) ^a	0.0204 \pm 0.0009
a/R_\star	22.65 \pm 0.50
ζ/R_\star	13.44 \pm 0.04
R_p/R_\star	0.1238 \pm 0.0009
b^2	0.097 ^{+0.032} _{−0.034}
$b \equiv a \cos i/R_\star$	0.311 ^{+0.046} _{−0.067}
i (deg)	89.2 ^{+0.2} _{−0.1}
Limb-darkening coefficients ^b	
c_1, i (linear term)	0.3592
c_2, i (quadratic term)	0.2759
c_1, z	0.2843
c_2, z	0.2882
c_1, I	0.3347
c_2, I	0.2800
RV parameters	
K (m s ^{−1})	58.4 \pm 0.9
k_{RV}^c	−0.321 \pm 0.006
h_{RV}^c	−0.129 \pm 0.013
e	0.346 \pm 0.007
ω (deg)	201 \pm 2
RV jitter (m s ^{−1})	2.3
Secondary eclipse parameters	
T_s (BJD)	2454804.246 \pm 0.037
$T_{s,14}$	0.1326 \pm 0.0036
$T_{s,12}$	0.0154 \pm 0.0007
Planetary parameters	
M_p (M_J)	0.530 \pm 0.018
R_p (R_J)	1.010 \pm 0.029
$C(M_p, R_p)$ ^d	0.44
ρ_p (g cm ^{−3})	0.64 \pm 0.05
$\log g_p$ (cgs)	3.11 \pm 0.02
a (AU)	0.0882 \pm 0.0014
T_{eq} (K)	792 \pm 15
Θ^e	0.108 \pm 0.004
F_{per} (10 ⁸ erg s ^{−1} cm ^{−2}) ^f	1.95 \pm 0.15
F_{ap} (10 ⁷ erg s ^{−1} cm ^{−2}) ^f	4.60 \pm 0.36
$\langle F \rangle$ (10 ⁷ erg s ^{−1} cm ^{−2}) ^f	8.89 \pm 0.66

^a T_c : Reference epoch of mid transit that minimizes the correlation with the orbital period. It corresponds to $N_{tr} = -32$. T_{14} : total transit duration, time between first to last contact; $T_{12} = T_{34}$: ingress/egress time, time between first and second, or third and fourth contact.

^b Values for a quadratic law, adopted from the tabulations by Claret (2004) according to the spectroscopic (SME) parameters listed in Table 4.

^c Lagrangian orbital parameters derived from the global modelling, and primarily determined by the RV data.

^d Correlation coefficient between the planetary mass M_p and radius R_p .

^e The Safronov number is given by $\Theta = \frac{1}{2}(V_{\text{esc}}/V_{\text{orb}})^2 = (a/R_p)(M_p/M_\star)$ (see Hansen & Barman 2007).

^f Incoming flux per unit surface area, averaged over the orbit.

on the exact molecule. TiO absorption has been suggested by Hubeny et al. (2003) while Zahnle et al. (2009) argue that sulfur photochemistry is key to generating an atmospheric temperature inversion. HAT-P-17 is a chromospherically quiet star with $\log R'_{\text{HK}} = -5.039$. Thus, the activity-inversion relation predicts that the atmosphere of HAT-P-17b will be inverted. The two host stars in the Knutson, Howard, & Isaacson (2010) sample with

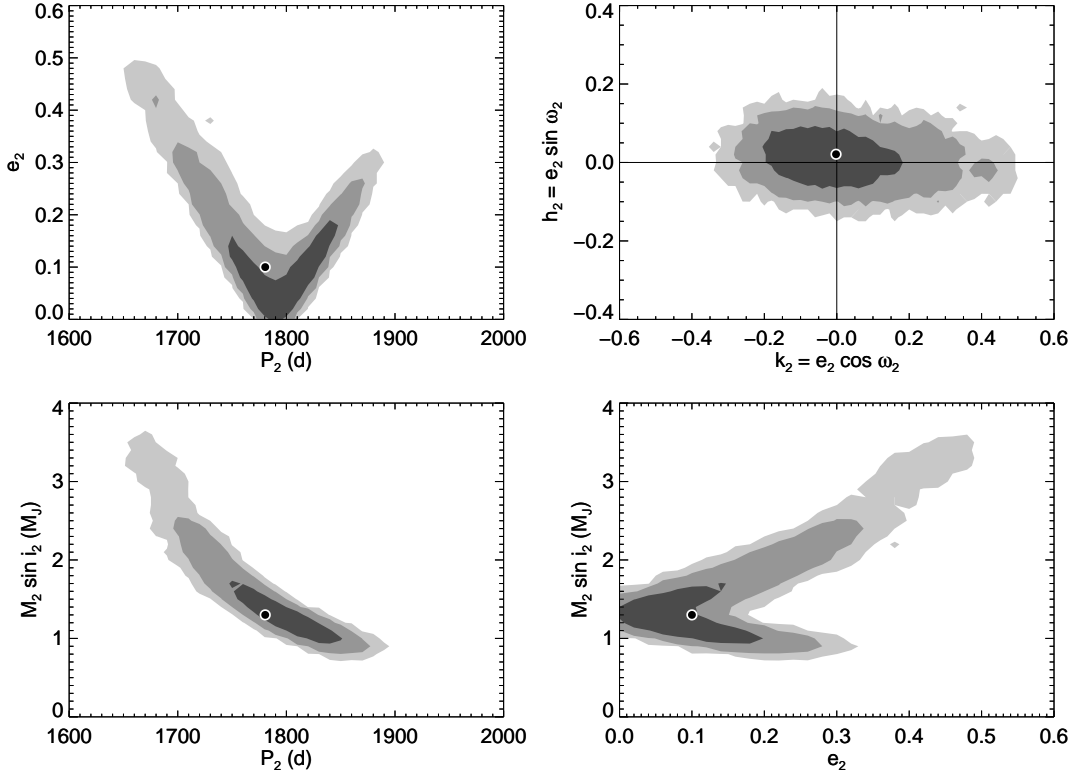


FIG. 5.— *A posteriori* distributions showing correlations between parameters describing HAT-P-17c. Best-fit parameter values are marked with filled circles. Grayscale regions enclose 68.3%, 95.4%, and 99.73% of the MCMC samples.

properties most similar to HAT-P-17—WASP-2 ($T_{\text{eff}} = 5230\text{ K}$, $\log R'_{\text{HK}} = -5.054$) and XO-2 ($T_{\text{eff}} = 5340\text{ K}$, $\log R'_{\text{HK}} = -4.988$)—both have planets with measured temperature inversions.

A key caveat is that the activity-inversion relation is based on a sample of relatively hot planetary atmospheres. The photochemistry responsible for atmospheric temperature inversion may not be active on the relatively cool HAT-P-17b ($T_{\text{eq}} = 792\text{ K}$). For example, the sulfur photochemistry model by Zahnle et al. (2009) is only active for $T \geq 1200\text{ K}$. Observations of this planet in secondary eclipse will probe the temperature range over which such inversions are produced and may offer clues to the identity of the absorbing molecules.

We computed the signal-to-noise ratios (SNR) of warm *Spitzer* secondary eclipse observations of HAT-P-17b assuming either efficient day-night circulation ($T_{\text{eq}} = 780\text{ K}$) or a hot day side with no circulation ($T_{\text{eq}} = 927\text{ K}$). For this range of atmospheres, we estimate that *Spitzer* will measure the secondary eclipse depth with $\text{SNR} = 2\text{--}5$ at $3.6\text{ }\mu\text{m}$ and $\text{SNR} = 3\text{--}6$ at $4.5\text{ }\mu\text{m}$ for an observation of a single secondary eclipse. This sensitivity will help constrain atmosphere models for this planet. The superior collecting area and extended IR coverage of *JWST* will give significantly stronger constraints on the IR emission spectrum of HAT-P-17b.

4.1.2. Spin-orbit Alignment

In the core accretion theory of planet formation, hot giant planets like HAT-P-17b form beyond the ice line (a few AU from the host star) and subsequently

migrate inward. Several migration mechanisms have been proposed. Tidal interactions with the protoplanetary disk (Lin et al. 1996) deliver gas giants with uniformly low obliquity. Alternatively, Kozai cycles (Fabrycky & Tremaine 2007) or planet-planet scattering (Chatterjee et al. 2009) leave the migrated planets in high obliquity orbits, possibly with high eccentricity (depending on the degree of tidal damping). Both high and low-obliquity systems have been observed by the Rossiter-McLaughlin (R-M) effect, suggesting some combination of migration mechanisms (Fabrycky & Winn 2009; Morton & Johnson, in preparation).

Winn et al. (2010) recently noted that nearly all misaligned (high obliquity) planets orbit hot stars ($T_{\text{eff}} > 6250\text{ K}$). They suggested that all hot giant planets migrated by one of the high obliquity mechanisms and that planets orbiting cool stars subsequently align the spin axis of the convective zones and photospheres of their hosts with the orbital plane. Stars above this threshold temperature lack a significant convective zone and their close-in giant planets remain in high-obliquity orbits.

Although HAT-P-17 is a cool star, the Winn et al. model predicts spin-orbit misalignment because the wider, eccentric orbit of HAT-P-17b lengthens the timescale for orbital decay considerably. Of the known TEPs, HAT-P-17b has the longest expected timescale except for HD 80606b (J. Winn, personal communication). In particular, HAT-P-17b has a longer timescale than WASP-8b, which is known to be misaligned (Queloz et al. 2010). This planet ($P = 8\text{ d}$, $e = 0.31$) is broadly similar to HAT-P-17b and also orbits

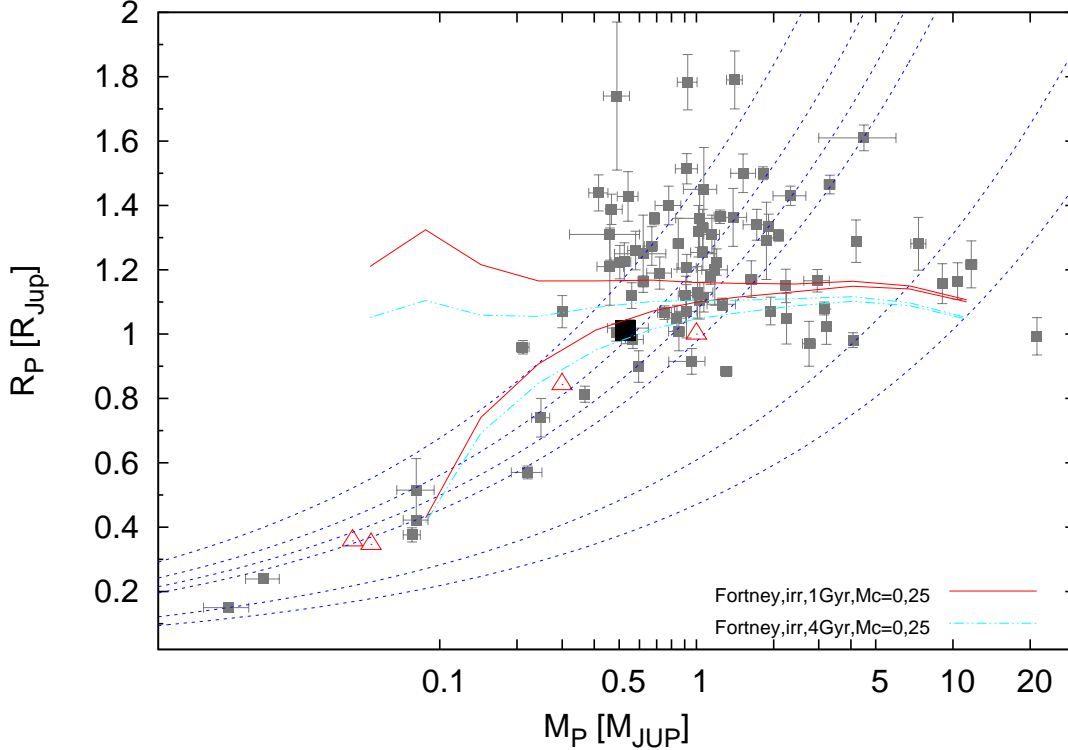


FIG. 6.— Mass-radius diagram of known TEPs (small filled squares). HAT-P-17b is shown as a large filled square. Overlaid are Fortney et al. (2007) planetary isochrones interpolated to the solar equivalent semi-major axis of HAT-P-17b for ages of 1.0 Gyr (upper solid lines) and 4 Gyr (lower dashed-dotted lines) and core masses of 0 and $25 M_{\oplus}$ (upper and lower lines respectively), as well as isodensity lines for 0.4, 0.7, 1.0, 1.33, 5.5 and $11.9\ g\ cm^{-3}$ (dashed lines). Solar system planets are shown with open triangles.

a relatively cool star ($T_{\text{eff}} = 5600\ K$).

Measuring the projected spin-orbit angle λ of HAT-P-17b is a challenging but plausible proposition with HIRES. We estimate a $4\text{--}11\ m\ s^{-1}$ amplitude R-M effect for $v \sin i = 0.3\text{--}0.8\ km\ s^{-1}$.

4.1.3. Similarity to HAT-P-15b

HAT-P-17b is strikingly similar to HAT-P-15b (Kovács et al. 2010) in orbital period (10.3 d and 10.9 d, respectively) and eccentricity (0.35 and 0.19, respectively). The mass of HAT-P-15b is significantly larger though ($0.5 M_J$ and $1.9 M_J$, respectively). These two planets are the only ground-based transit discoveries with orbital periods longer than 10 d. (Other transiting planets with $P > 10\ d$ include those detected by space-based transit surveys and two planets discovered by RVs that were later shown to transit.) The bias toward detecting planets with short orbital periods with ground-based transit searches stems from the observational window function of a longitudinally-spaced multi-site telescope network (von Braun, Kane, & Ciardi 2009). The HAT-South survey will significantly improve the detection of longer period transiting planets with a 50% detection rate out to orbital periods of 12 d (Bakos et al. 2009).

4.2. Transit Timing Variations

The presence of a second detected planet in the HAT-P-17 system raises the possibility of transit timing variations (TTVs; Holman & Murray 2005). However, because HAT-P-17b and HAT-P-17c are widely separated

($a_2/a_1 \sim 31$) and HAT-P-17c is on a nearly circular orbit, the two planets interact very weakly. The TTVs are expected to be less than 1 s, undetectable with current techniques.

4.3. The Planet HAT-P-17c

HAT-P-17c is an approximately Jupiter-mass planet separated from its host star by about half the Sun-Jupiter separation. Despite having only observed 50% of the orbit of HAT-P-17c, its orbital parameters are well constrained for a long-period planet (Figure 5). While we cannot completely rule out a highly eccentric orbit, only 3% of the MCMC samples have $e > 0.3$.

The 2007 Dec 14 light curve (Figure 3) showing a partial transit of HAT-P-17b is during the broad transit window of HAT-P-17c. We interpret the detected transit as due to HAT-P-17b because the timing precisely matches the ephemeris derived from other transits. We do not detect additional transits (possibly due to HAT-P-17c) in that light curve. Because that light curve is the only one taken in z-band we cannot compare the photometric level of this transit with others to see if it was taken entirely when HAT-P-17c was in transit.

Based on the current orbital fit, the next opportunity to search for a transit of HAT-P-17c is in 2012 Oct. The timing is favorable for an observing campaign as the star is visible for $\sim 5\ hr$ per night from mid-Northern latitudes. From the ground, a coordinated, multi-site search spanning a range of longitudes is likely necessary to rule in or out $\sim 1\%$ deep transits of maximum duration

TABLE 6
ORBITAL AND PLANETARY PARAMETERS FOR HAT-P-17c

Parameter	Value
RV parameters, as induced by HAT-P-17c	
P_2 (days)	1798^{+58}_{-89}
T_{2c}^a (BJD)	2452636 ± 58
K_2 (m s^{-1})	25^{+24}_{-6}
k_2	$0.00^{+0.32}_{-0.22}$
h_2	$0.02^{+0.10}_{-0.09}$
e_2	$0.10^{+0.23}_{-0.10}$
ω_2	$155 \pm 150^\circ$
$T_{2,peri}$ (days)	2452670 ± 702
Hypothetical light curve parameters, HAT-P-17c ^b	
$T_{2,14}^c$ (days)	0.883 ± 0.092
$T_{2,12} = T_{34}$ (days)	0.1008 ± 0.0114
Hypothetical secondary eclipse parameters for HAT-P-17c ^a	
T_{2s} (BJD)	2453531 ± 208
$T_{2s,14}$ (days)	0.92 ± 0.11
$T_{2s,12}$ (days)	0.101 ± 0.011
Planetary parameters for HAT-P-17c	
$m_2 \sin i_2$ (M_J)	$1.4^{+1.1}_{-0.4}$
a_2 (AU)	2.75 ± 0.12
$T_{2,eq}$ (K)	140 ± 6
$F_{2,per}$ ($10^5 \text{ erg s}^{-1} \text{ cm}^{-2}$) ^d ..	1.1 ± 0.5
$F_{2,ap}$ ($10^4 \text{ erg s}^{-1} \text{ cm}^{-2}$) ^d ...	7.0 ± 1.8
$\langle F_2 \rangle$ ($10^4 \text{ erg s}^{-1} \text{ cm}^{-2}$) ^d	8.7 ± 1.2

^a T_{2c} would be the center of transit of HAT-P-17c, if its (unknown) inclination is 90° .

^b Transits of HAT-P-17c have not been observed. The values are for guidance only, and assume zero impact parameter.

^c T_{14} : total transit duration, time between first to last contact, assuming zero impact parameter. $T_{12} = T_{34}$: ingress/egress time, time between first and second, or third and fourth contact. Note that these values are hypothetical, and transits of HAT-P-17c have not been observed.

^d Incoming flux per unit surface area in periastron, apastron, and averaged over the orbit.

0.883 d.

4.4. Planet Multiplicity

The migration mechanism of hot jovian planets remains a major outstanding problem of planet formation and evolution. The presence of additional massive planets in a system points to migration within the protoplanetary disk, while the absence of additional planets suggests a more disruptive mechanism such planet-planet scattering or the Kozai mechanism.

Wright et al. (2009) measured the rate of planet multiplicity and found that 14% of exoplanet host stars are multi-planet systems and another 14% show evidence of

multiplicity in the form of an RV trend. Here we compute the fraction of stars hosting a “cool jovian planet” ($m \sin i > 0.2 M_J$ and $a > 0.2 \text{ AU}$) that also host a “hot jovian planet” ($m \sin i > 0.2 M_J$ and $a < 0.2 \text{ AU}$). We used the Exoplanet Orbit Database¹³ of planets with well-defined orbital parameters. Of the 375 planet hosts (including HAT-P-17), we find 106 stars that host a hot jovian planet and 204 stars that host one or more cool jovian planets. Of the latter group, 10 stars (5%) also host a hot jovian planet. Restricting the hot jovian planets to $a < 0.1 \text{ AU}$, $6/204 = 3\%$ of stars host both cool and hot

¹³ <http://exoplanets.org>

jovian planets. Note that this selection of planets does not suffer from a significant detection bias; the Doppler signal from a hot jovian planet is essentially always detectable for systems with a detected cool jovian planet. While hot jovian planets represent a disproportionately large fraction of the known planets due to observational selection effects, multi-planet systems like HAT-P-17 are rare.

We thank H. Knutson, J. Winn, and J. Wright for helpful conversations. HATNet operations have been funded by NASA grants NNG04GN74G, NNX08AF23G and SAO IR&D grants. A.W.H. gratefully acknowledges support from a Townes Post-doctoral Fellowship at the U. C. Berkeley Space Sciences Laboratory. Work of G.Á.B. and J. Johnson were supported by the Postdoctoral Fellowship of the NSF Astronomy and Astrophysics Program (AST-0702843 and AST-0702821, respectively). G.T. acknowledges partial support from NASA grant NNX09AF59G. We acknowledge partial support also from the Kepler Mission under NASA Cooperative Agreement NCC2-1390 (D.W.L., PI). G.K. thanks the Hungarian Scientific Research Foundation (OTKA) for support through grant K-81373. T.M. acknowledges the Israel Science Foundation (grant 655/07). This research has made use of Keck telescope time granted through NOAO and NASA. We thank Ezra Mashal for his help in operating the Wise HAT telescope over the past years. We thank the TLC project (M. Holman and J. Winn) for swapping time on the 1.2 m telescope on a short notice. This research has made use of the Exoplanet Orbit Database and the Exoplanet Data Explorer at exoplanets.org, the SIMBAD database (operated at CDS, Strasbourg, France), and NASA’s Astrophysics Data System Bibliographic Services. Finally, the authors wish to extend special thanks to those of Hawai’ian ancestry on whose sacred mountain of Mauna Kea we are privileged to be guests. Without their generous hospitality, the Keck observations presented herein would not have been possible.

REFERENCES

- Bakos, G. Á., Noyes, R. W., Kovács, G., Staneek, K. Z., Sasselov, D. D., & Domsa, I. 2004, *PASP*, 116, 266
 Bakos, G. Á., et al. 2007, *ApJ*, 670, 826
 Bakos, G. Á., et al. 2009, *IAU Symposium*, 253, 354
 Bakos, G. Á., et al. 2010, *ApJ*, 710, 1724
 Bakos, G. Á., et al. 2010, *ApJ*, 707, 446
 Baraffe, I., Chabrier, G., Barman, T. S., Allard, F., & Hauschildt, P. H., *A&A*, 402, 701
 Baraffe, I., Chabrier, G., & Barman, T. 2008, *A&A*, 482, 315
 Batalha, N. M. 2010, *ApJ*, 713, L109
 Borucki, W. J. et al. 2010, , *ApJ*, submitted, arXiv:1006.2799B
 Bouchez, F., et al. 2005, *A&A*, 444, L15
 Buchhave, L. A., et al. 2010, *ApJ*, submitted, arXiv:1005.2009
 Butler, R. P. et al. 1996, *PASP*, 108, 500

- Butler, R. P., Vogt, S. S., Marcy, G. W., Fischer, D. A., Wright, J. T., Henry, G. W., Laughlin, G., & Lissauer, J. J. 2004, *ApJ*, 617, 580
- Carpenter, J. M. 2001, *AJ*, 121, 2851
- Casagrande, L., Portinari, L., & Flynn, C. 2006, *MNRAS*, 373, 13
- Charbonneau, D., Brown, T. M., Latham, D. W., & Mayor, M. 2000, *ApJ*, 529, L45
- Charbonneau, D., et al. 2009, *Nature*, 462, 891
- Chatterjee, S., et al. 2009, *ApJ*, 686, 580
- Claret, A. 2004, *A&A*, 428, 1001
- Droege, T. F., Richmond, M. W., & Sallman, M. 2006, *PASP*, 118, 1666
- Fabrycky, D., & Tremaine, S. 2007, *ApJ*, 669, 1298
- Fabrycky, D. C., & Winn, J. N. 2009, *ApJ*, 696, 1230
- Ford, E. 2006, *ApJ*, 642, 505
- Fortney, J. J., Marley, M. S., & Barnes, J. W. 2007, *ApJ*, 659, 1661
- Gillon, M., et al. 2007, *A&A*, 472, L13
- Hansen, B. M. S., & Barman, T. 2007, *ApJ*, 671, 861
- Hebb, L., et al. 2009, *ApJ*, 693, 1920
- Henry, G. W., Marcy, G. W., Butler, R. P., & Vogt, S. S. 2000, *ApJ*, 529, L41
- Holman, M. J., & Murray, N. W. 2005, *Science*, 307, 1288
- Howard, A. W., et al. 2010, *ApJ*, submitted, arXiv:1003.3444H
- Hubeny, I., Burrows, A., & Sudarsky, D. 2003, *ApJ*, 594, 1011
- Isaacson, H. & Fischer, D. A. 2010, *ApJ*, submitted
- Knutson, H. A. and Howard, A. W. and Isaacson, H. 2010, *ApJ*, accepted, arXiv:1004.2702K
- Kovács, G., Zucker, S., & Mazeh, T. 2002, *A&A*, 391, 369
- Kovács, G., Bakos, G. Á., & Noyes, R. W. 2005, *MNRAS*, 356, 557
- Kovács, G., et al. 2010, *ApJ*, submitted, arXiv:1005.5300
- Latham, D. W. 1992, in *IAU Coll. 135, Complementary Approaches to Double and Multiple Star Research*, ASP Conf. Ser. 32, eds. H. A. McAlister & W. I. Hartkopf (San Francisco: ASP), 110
- Lin, D. N. C. and Bodenheimer, P. and Richardson, D. C. 1996 *Nature*, 380, 606
- Léger, A. et. al. 2009, *A&A*, 506, 287
- Pál, A., & Bakos, G. Á. 2006, *PASP*, 118, 1474
- Pál, A. 2009, *MNRAS*, 396, 1737
- Pál, A. 2009b, arXiv:0906.3486, PhD thesis
- Perryman, M. A. C., et al., 1997, *A&A*, 323, 49
- Press, W. H., Teukolsky, S. A., Vetterling, W. T. & Flannery, B. P., 1992, *Numerical Recipes in C: the art of scientific computing*, Second Edition, Cambridge University Press
- Mandel, K., & Agol, E. 2002, *ApJ*, 580, L171
- Marcy, G. W., & Butler, R. P. 1992, *PASP*, 104, 270
- McLaughlin, D. B. 1924, *ApJ*, 60, 22
- Pál, A., et al. 2008, *ApJ*, 680, 1450
- Ramírez, I., & Meléndez, J. 2005, *ApJ*, 626, 465
- Queloz, D. et al. 2009, *A&A*, 506, 303
- Queloz, D. et al. 2010, *A&A*, 517, 1
- Shporer, A., Bakos, G. Á., Mazeh, T., Kovács, G., & Sipöcz, B. 2009, *IAU Symposium*, 253, 331
- Skrutskie, M. F., et al. 2006, *AJ*, 131, 1163
- Sozzetti, A. et al. 2007, *ApJ*, 664, 1190
- Steffen, J. H. et al. 2010, *ApJ*, submitted, arXiv:1006.2763
- Tingley, B., & Sackett, P. D. 2005, *ApJ*, 627, 1011
- Torres, G., Neuhäuser, R., & Guenther, E. W. 2002, *AJ*, 123, 1701
- Torres, G. et al. 2007, *ApJ*, 666, 121
- Valenti, J. A., & Fischer, D. A. 2005, *ApJS*, 159, 141
- Valenti, J. A., & Piskunov, N. 1996, *A&AS*, 118, 595
- Valenti, J. A., Butler, R. P., & Marcy, G. W. 1995, *PASP*, 107, 966
- Vogt, S. S. et al. 1994, *Proc. SPIE*, 2198, 362
- Vaughan, A. H., Preston, G. W., & Wilson, O. C. 1978, *PASP*, 90, 267
- von Braun, K., Kane, S. R., & Ciardi, D. R. 2009, *ApJ*, 702, 779
- Winn, J. N., Fabrycky, D., Albrecht, S., & Johnson, J. A. 2010, *ApJ*, 718, L145
- Wright, J. T. 2005, *PASP*, 117, 657
- Wright, J. T. et al. 2009, *ApJ*, 693, 1084
- Wu et al. 2007 *ApJ*, 670, 820
- Yi, S. K. et al. 2001, *ApJS*, 136, 417
- Zahnle, K. et. al. 2009, *ApJ*, 701, L20